Journal of Dentistry 132 (2023) 104500

Contents lists available at ScienceDirect

Journal of Dentistry

journal homepage: www.elsevier.com/locate/jdent

Impact of angle on photothermal radiometry and modulated luminescence (PTR/LUM) value

Haixia Xing [a,b], George J. Eckert [c], Masatoshi Ando [b,*]

[a] Department of General Dentistry, Peking University School and Hospital of Stomatology, Beijing, China
[b] Department of Cariology, Operative Dentistry and Dental Public Health, Indiana University School of Dentistry, 1121 W. Michigan Street, Indianapolis, IN 46202, USA
[c] Department of Biostatistics and Health Data Science, Indiana University School of Medicine, Indianapolis, IN, USA

ARTICLE INFO

Keywords:
Dental caries
Tooth demineralization
Early diagnosis
Dental enamel
Optical device
Scanning angle

ABSTRACT

Objective: To evaluate the impact of scanning angles to detect/quantify non-cavitated caries by photothermal-radiometry and modulated-luminescence (PTR/LUM, Canary System) and to evaluate the association of PTR/LUM value with lesion depth (LD), including sound tissue thickness under the lesion (ST).
Methods: Thirty human extracted premolars were selected based on micro-computed tomography [μ-CT: sound (n=12), lesions into outer-half of enamel (n=6), lesions into inner-half of enamel (n=6), lesions into outer one-third of dentine (n=6)]. Each tooth sample was scanned 90° directly contacted to the center of non-cavitated lesion or sound smooth surface, and tilted 10° and 20° in four directions: buccal/lingual/occlusal/cervical. The procedure was repeated 48 h later. Lesion depth and ST [ST=5000 μm (maximum PTR/LUM scanning depth)-LD] were measured at the same scanning direction on μ-CT images. Sensitivity, specificity, area under the Receiver Operating Characteristic curve (AUC), and intraclass correlation coefficients (ICC) for different scanning angles were calculated. Sensitivity was further evaluated based on lesion extensions. Relationships between PTR/LUM value and lesion depth, and between PTR/LUM value and LD/ST-Ratio were evaluated.
Results: PTR/LUM value showed significant differences among scanning angles. Overall sensitivity (78%–89%), specificity (66%–87%), AUC (0.86–0.92) and ICC (0.89–0.99), sensitivity based on lesion extensions presented no significant differences among angles. PTR/LUM value showed moderate correlations (0.56–0.74) with deepest lesion depth and LD/ST-Ratios.
Conclusion: The scanning angle within 20° increments might impact PTR/LUM value statistically; however, it did not affect PTR/LUM detection performance. PTR/LUM values were positively correlated with non-cavitated lesion depth, and not affected by sound tissue thickness under the lesion.
Clinical significance: : Clinically, it is challenging to measure/scan at the same location and same angle longitudinally, however, it is important to standardize these parameters. Scanning within 20° deviation from perpendicular did not affect detection performance of PTR/LUM, and PTR/LUM value showed positive moderate correlation with caries depth.

1. Introduction

The optical properties of the dental hard tissues can be described as optical constants (absorption and scattering coefficients), which are different for sound tissue and dental caries [1]. When a modulated red laser at 660 nm strikes on the tooth surface, light interaction with the tooth surface generates thermal energy radiation (heat response raising about one degree Celsius) and luminescence energy radiation (light response) [2,3]. The photothermal radiometry and modulated luminescence (PTR/LUM) technology analyzes the response of the thermal behavior and reemitted radiation (luminescence) of the emitted infrared photons simultaneously, providing information on the depth and degree of tooth demineralization [4]. PTR/LUM is a potential technique for caries detection clinically, which was demonstrated by a multi-center clinical evaluation [5]. PTR/LUM's sensitivity was much higher than visual examination or radiographs when detecting occlusal fissures caries [6,7], displayed higher sensitivity (93.3%) than bitewing radiographs *in vitro* [8], and comparable [9] even much higher sensitivity [10] than bitewing radiographs when detecting approximal caries *in vivo*. For non-cavitated dental caries detection, the 61% sensitivity to

* Corresponding author.
E-mail address: mando@iu.edu (M. Ando).

https://doi.org/10.1016/j.jdent.2023.104500
Received 11 November 2022; Received in revised form 10 March 2023; Accepted 22 March 2023

detect non-cavitated approximal caries with adjacent teeth existing [11] and 85% sensitivity to detect non-cavitated occlusal caries [12] showed the ability of PTR/LUM in detecting non-cavitated dental caries.

When using any dental caries detection technique, it is important to standardize parameters, such as the scanning angle. PTR/LUM provides accurate analysis of the dental crystal structure based on the concept of "point scanning." The PTR/LUM manufacturer recommends to scan the region of interest perpendicular to the surface. Even the slightest adjustment in hand piece angulation can result in scanning a different area of the tooth [12,13]. Large standard deviations for PTR/LUM value were shown for the scan performed at varying angles [9]. Despite training and calibration done prior to examination, examiners still found PTR/LUM values were affected by the scanning angle [12]. How the scanning angle impacts the PTR/LUM value was not documented clearly.

PTR/LUM values directly link to the status of tooth mineralization and crystallization using a numerical scale [4,14]. PTR/LUM values were affected by lesion depth, the volume of demineralized tissue, thickness and integrity of the overlying surface layer [7]. In the application of PTR/LUM, lesion depth information was obtained following optical-to-thermal energy conversion and transport of the incident laser power conductively and radiatively [6,15]. PTR/LUM values were correlated with artificial lesion depth [3,16]. For natural lesions, the decay zone (PTR/LUM value: 21–70) might indicate lesions depth of 532 ±322 μm (mean ± standard deviation), and the advanced decay zone (PTR/LUM value: 71–100) might indicate lesions depth of 1057±441 μm [7]. One limitation of this study was that only twenty scanning sites were included. To the authors' knowledge, no other study has thus far validated the relationship between PTR/LUM value and natural caries lesion severity. These drived further research to evaluate the correlation between PTR/LUM value and natural lesion depth. When PTR/LUM scans an artificial non-cavitated caries lesion, the healthy crystal tissue beneath the lesion might decrease PTR amplitude and LUM phase [17], which might change PTR/LUM value. Quantitative evaluation of sound tissue thickness under lesions contributing to PTR/LUM value is also needed.

Therefore, the objectives of this study were to assess: (1) the impact of varying scanning angles to detect and quantify non-cavitated natural caries by PTR/LUM; and (2) the associations of lesion depth and sound tissue thickness under the lesion with PTR/LUM value. Our hypotheses were increasing scanning angle decreases the PTR/LUM value, PTR/LUM value positively correlates with lesion depth, but negatively correlates with sound tissue thickness under the lesion.

2. Materials and methods

2.1. Teeth samples selection

Fifty human extracted premolars were selected, with sound to non-cavitated lesions on approximal surfaces, to simulate smooth surface caries, as similar manner as prescribed earlier [18]. The teeth were collected from dental practitioners s in local area (USA), transported in 0.1% thymol solution and then stored in an air-tight humid container at 4 °C. The collection of human teeth for use in dental laboratory research had been approved by the Institutional Review Board (IRB #NS0911-07). Before the study, all teeth samples were cleaned with Robinson's brush under water on a slow speed rotary handpiece to remove any debris or adhering soft tissue.

2.2. Initial micro-computed tomography (μ-CT) image acquisition

The teeth samples were mounted and secured on Lego® bricks (The LEGO Group, Billund, Denmark) using utility wax (Heraeus Kulzer Inc., Lafayette, IN, USA). The μ-CT images were acquired using a Skyscan μ-CT instrument (Skyscan 1172, Kontich, Belgium) at 80 kV, 134μe, 8.9 μm pixel size resolution with an Al + Cu filter. NRecon version 1.6.6 software (Bruker microCT, Kontich, Belgium) was used to reconstruct a two-dimensional (2D) image. With image display software (CT-Analyser, Bruker microCT, Kontich, Belgium), the axial views of the 2D images were observed and scored by two experienced examiners independently. The deepest lesion extension was determined. In case of disagreement, the examinations were performed again until consensus agreement was achieved. From the fifty teeth samples, thirty premolars with/without non-cavitated lesion on the approximal surface were selected for this study. The final distribution of the 30 study teeth samples was as follows: sound surface (μ-CT=0: n=12), lesion in the outer half of the enamel (μ-CT=1: n=6), lesion in the inner half of the enamel but not extending beyond the dentin-enamel junction (μ-CT=2: n=6), and lesions in the outer one third of the dentin (μ-CT=3: n=6).

2.3. Model assembly and second μ-CT image acquisition

The selected study teeth samples were placed on plastic Lego® bricks using Triad® visible light cure resin (DENTSPLY International, Inc., York, USA) around the root up to the cervical part to secure the teeth samples. To confirm the lesion depth and acquire standardized μ-CT images as gold standard, study teeth samples were scanned again using μ-CT as described in *Initial μ-CT image acquisition*. The assembled models were kept in a container with wet gauze to maintain humidity.

2.4. Location of the region of interest

To locate the region of interest, all approximal smooth surfaces were photographed along with a ruler using a light stereomicroscope (DSM, Nikon-SMZ1500; Nikon Inc., Tokyo, Japan). When a non-cavitated lesion was visible, the region of interest was determined at the center of lesion by the distances from lesion center point to buccal cusp and buccal surface using Microsoft Paint (Microsoft® Paint® version 6.1, Microsoft Corporation, Redmond, WA, USA). When the non-cavitated lesion was not visible, the region of interest was located at the center of the approximal surface measured by the distances to buccal cusp and buccal surface.

2.5. PTR/LUM examination at different scanning angles

Teeth samples were scanned on the region of interest by PTR/LUM (Canary System®, Quantum Dental Technologies, Toronto, Ont., Canada) following the manufacturer's instructions. Teeth samples were placed on the metric goniometer (60 MM GONIOMETER, 40°, Edmund Optics America, NJ, USA). The wavelength of PTR/LUM was 660±10 nm with fixed frequency (2 Hz) modulation, at 50% duty cycle. PTR/LUM technique captures signals from a hemispherical area beneath the laser beam as wide as 1.5 mm in diameter up to a depth of 5 mm [7,19] (Fig. 1a). The PTR/LUM handpiece was fixed with a holder. The examiner, who was trained to perform PTR/LUM scanning, was independent from the one who selected study teeth samples. After calibration in accordance with the manufacturer's calibration instructions, each tooth sample was scanned under the disposable plastic tip on the handpiece, which was positioned 90° directly in contact to the center of lesion or sound surface following the instructions from the manufacturer's manual handbook. The handpiece was then tilted 10° and 20° in four directions: buccal, lingual, occlusal, and cervical with one side of the probe tip edge still contacting on the surface (Fig. 1a). For each scan, the PTR/LUM value was recorded. To evaluate intra examiner repeatability, all measurements were repeated 48 h later.

2.6. Measurement of the lesion depth and the sound tissue thickness under the lesions at different measuring angles

Dataviewer (Bruker microCT, Kontich, Belgium) software was used to determine the lesion depth (LD) and the sound tissue thickness under the lesion (ST) at different angles. Since the maximum scanning depth of

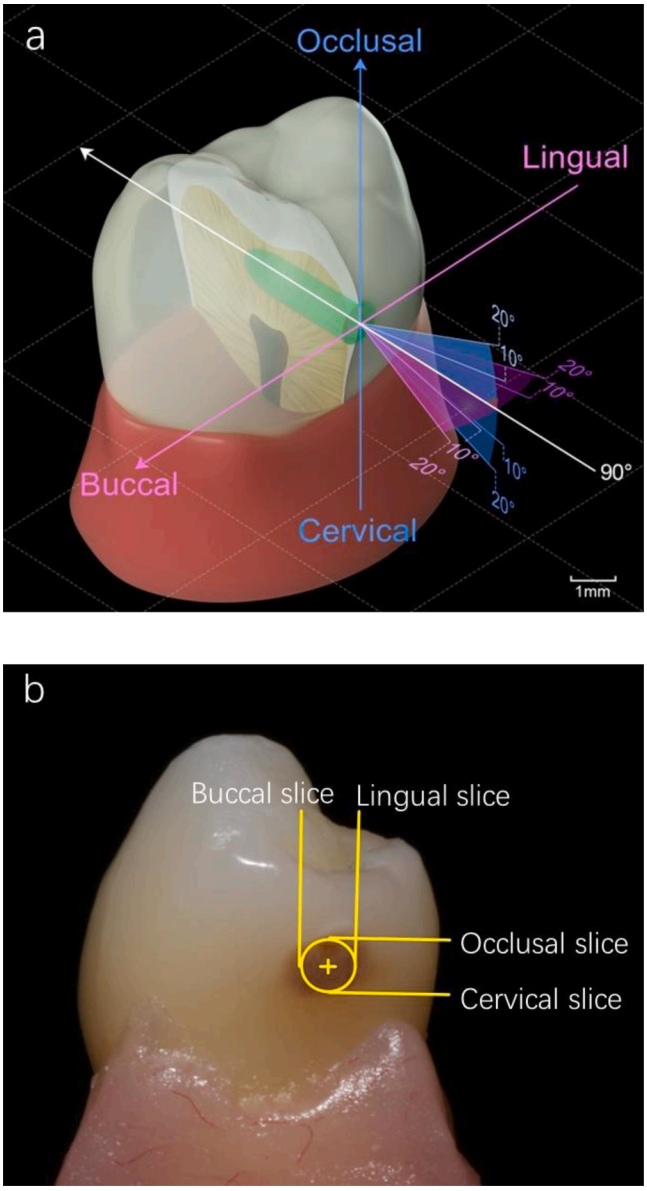

Fig. 1. Different scanning angles and locations of analysis. Fig. 1a: 3D model showing different scanning angles. Pink color indicates buccal-lingual direction; blue color indicates occlusal-cervical direction. Hemispherical green area shows laser beam penetrating into tissue. Fig. 1b: Locations of analyzing slices on μ-CT images. Circle indicates location of scanning area and "┼" shows center of laser beam and also center of analyzing slices on μ-CT images.

PTR/LUM is 5 mm=5000 μm [19], ST was determined as follow: ST=5000-LD. The ratio of lesion depth to sound tissue thickness under the lesion (LD/ST-Ratio) was calculated. The region of interest on μ-CT images was located by the central slice of the lesion boundary (Middle), and then 750 μm away from Middle in Buccal/Lingual/Occlusal/Cervical directions which were utilized as the scanning boundary because of the 750 μm radius of the PTR/LUM laser spot [19] (Fig. 1b). On each slice, lesion depth was measured perpendicular to region of interest [Buccal-Lingual 90°, Occlusal-Cervical 90°], and tilted 10° and 20° in four directions (Buccal, Lingual, Occlusal, Cervical).

2.7. Statistical analysis

Statistical analysis was performed at the following different angles: 20° to Buccal, 10° to Buccal, Buccal-Lingual 90°, 10° to Lingual, 20° to Lingual, 20° to Occlusal, 10° to Occlusal, Occlusal-Cervical 90°, 10° to Cervical, 20° to Cervical. For each angle, the PTR/LUM value, lesion depth, and LD/ST-Ratio were summarized, and intra class correlation coefficients (ICC) were calculated. Furthermore, sensitivity, specificity, and area under the ROC curve (AUC) were calculated and compared using bootstrap analyses. Sensitivity was further evaluated based on lesion extension. Pearson correlation coefficients for PTR/LUM value with lesion depth and LD/ST-Ratio were calculated to evaluate the association at different angles.

3. Results

Mean and standard deviation, minimum, median and maximum value for lesion depth and LD/ST-Ratio for each measuring angle on micro-CT images were shown in Fig. 2a and b. No significant differences among angles were found for mean lesion depth (p=0.15) or LD/ST-Ratio (p=0.11); however, there were some trends. For the buccal-lingual direction, mean and median lesion depth increased as measuring angle increased from 90°. For the occlusal-cervical direction, mean and median lesion depth increased as the scanning direction from cervical to occlusal.

For the sound surfaces (n=12), the mean PTR/LUM value was 20.6 (standard deviation: 1.3). For caries lesions (n=18), mean PTR/LUM values and standard deviations for each scanning angle were shown in Fig. 2c. PTR/LUM values were significantly different among scanning angles. For the buccal-lingual directions, the PTR/LUM values had a trend to increase as the angle increased. The maximum PTR/LUM value was found at 10° to cervical (56±27), significantly higher than buccal-lingual 90° (48±22) and occlusal-cervical 90° (51±25), and all other angles except 20° to cervical and 20° to lingual. The minimum PTR/LUM value was found at buccal-lingual 90° (48±22), significantly lower than 10° to cervical (56±27), 20° to cervical (54±28) and 20° to lingual (53±25).

Sensitivity, specificity, AUC, and ICC are presented in Table 1. Overall sensitivity ranged from 78%−89%, specificity 66%−87%, AUC 0.86–0.92 and ICC 0.89–0.99. There were no significant differences among angles for overall sensitivity (p≥0.12), sensitivity for different lesion extension μ-CT=1/μ-CT=2/μ-CT=3 (p≥0.10, p≥0.50, p=1.00), specificity (p≥0.06), AUC (p≥0.18), and ICC (p≥0.06).

Pearson correlation coefficients were calculated for PTR/LUM value with lesion depth (Table 2a) and LD/ST-Ratio (Table 2b). The highest correlations with either the mean or maximum lesion depth was found in the middle μ-CT slice (Pearson correlation coefficients 0.51–0.65), with similar correlations when using the maximum lesion depth across all slices, and slightly higher correlations with deepest lesion depth. Correlations were similar in Tables 2a and 2b, indicating that the thickness of sound tissue under the lesion did not appear to affect the association of PTR/LUM with lesion depth.

4. Discussion

Our hypotheses were partially supported by the results. The PTR/LUM technique collects the emitted infrared radiation (heat) and luminescence light upon interaction with the crystalline tissue of dental hard tissue. Thickness of the surface layer, scanning angle, lesion depth, and thickness of surrounding healthy tissue are some factors that may impact PTR/LUM values due to different optical (absorption and scattering) coefficients and thermophysical parameters, spectrally averaged infrared emissivity, thermal diffusivity and conductivity [20,21]. This current study demonstrated that scanning angles within 20° from perpendicular to the surface might impact PTR/LUM values; however, they may not affect PTR/LUM detection performance. Lesion depth, especially the deepest lesion depth for all slices, was significantly correlated with PTR/LUM value. The sound tissue thickness under the lesion did not impact the correlation of PTR/LUM value with lesion depth.

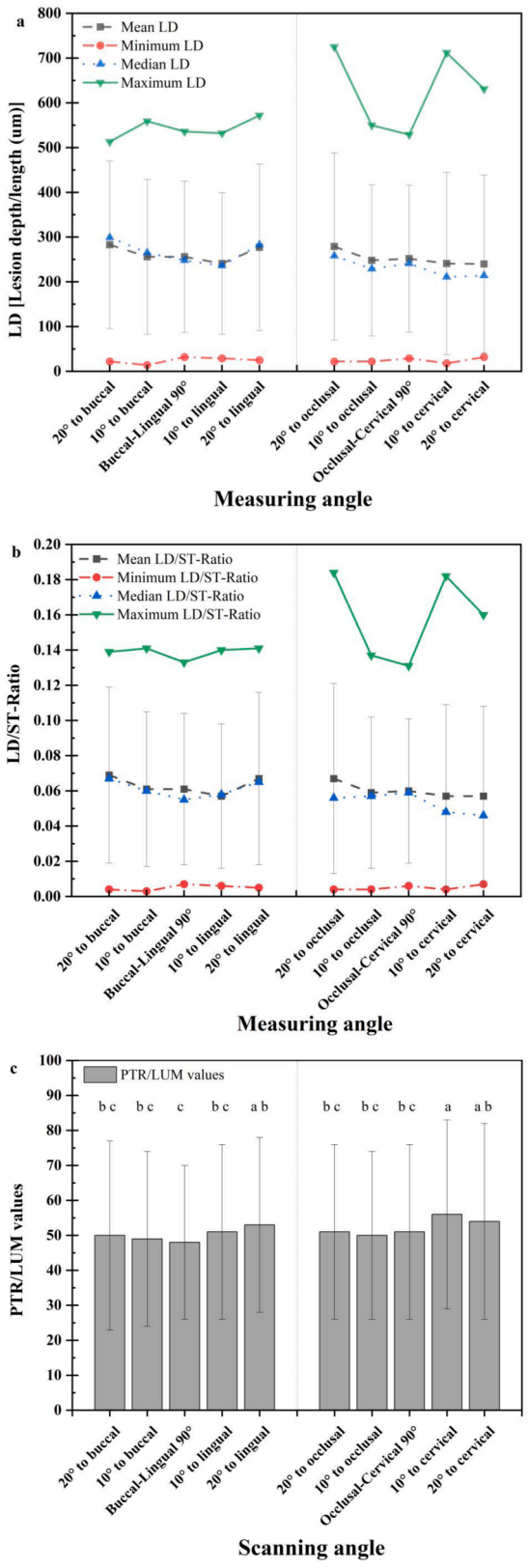

Fig. 2. Mean±standard deviation, minimum, median and maximum for lesion depth (LD, Fig. 2a), lesion depth/sound tissue length under lesion (LD/ST-Ratio, Fig. 2b) for measuring angle, and mean PTR/LUM values±standard deviation (Fig. 2c) for each scanning angle. No significant differences were found among angles for mean lesion depth ($p=0.15$) or mean LD/ST-Ratio ($p=0.11$). For PTR/LUM values, same letters indicate no significant difference among angles ($p<0.05$).

4.1. Impact of varying scanning angle on PTR/LUM value

When detecting non-cavitated caries, the dominant contribution to PTR/LUM value was lesion depth [6]. Mineral loss increases the porosity of hard tissue and changes the optical properties, resulting in a corresponding increase in the PTR/LUM value [22,23]. The perception existed that the PTR/LUM technique was sensitive to scanning angle [12,13,21]. However, in this current study, the mean lesion depth showed no significant differences among angles in the enrolled teeth samples. Therefore, the results that different scanning angles impact on PTR/LUM value might be due to the orientation and direction of demineralized enamel rods, not lesion depth.

It is well known that early mineral dissolution follows the direction of the enamel rods, then causes small changes in the enamel rods' ultrastissue [24]. Changes in PTR/LUM values accompanied by changes in optical constants and thermophysical parameters (spectrally averaged infrared emissivity, thermal diffusivity, and conductivity) [20]. The thermal wave (heat) diffusion length to surrounding areas depended on the material properties of the tooth crystal structure [21]. When scanning in the buccal-lingual direction, as scanning angle increased, PTR/LUM value also tended to increase. This can be explained by the nature of approximal non-cavitated caries. When approximal non-cavitated enamel caries is observed on a transverse plane (observed from the occlusal surface), the caries appears rectangular or 'kidney bean' shaped [25,26]. The orientation and direction of enamel rods on the transverse plane has been reported either aligned outward and toward the occlusal surface [27–29] or directed straight from the dentin-enamel junction to the external surface [30]. This implies that when the scanning angle increases, lesion depth might get deeper/longer, which results in PTR/LUM value increasing.

Scanning from the cervical direction showed larger PTR/LUM values. However, lesion depth from the cervical direction was not deeper than lesion depth from occlusal direction. This reflects the nature of approximal non-cavitated caries: on the coronal plane (observed from the facial/lingual surface), caries appears triangular with a wide area of origin and one vertex on the pulp side directed towards the cervical area [24]. The potential explanation for larger PTR/LUM values from the cervical direction could be the orientation and direction of demineralized enamel rods. At the approximal surface, the enamel rods were inclined to the long axis of the tooth at an acute angle ($60°\pm5°$) to the outer surface [31]. Scanning from the cervical direction, the light incidence angle to enamel rods is smaller than from the occlusal direction. Then light would hit to either the a- or b-axis of enamel rods. The distance is shorter than the c-axis, hence, light has less chance to scatter, but is more likely to refract. The amorphous crystalline disintegration would reduce scattering centers through the smaller number of crystal grain boundaries and smaller demineralized enamel crystals size. As a result, light and heat are confined to the region with crystalline disintegration because of the decreasing scattering coefficient and thereby create abundant thermal properties [32]. Finally, as stated earlier [21,32], the increasing generated PTR signals and decreasing LUM signals resulted in a corresponding increase in the PTR/LUM value from the cervical direction.

4.2. Impact of varying scanning angles on PTR/LUM performance

In the current study, sensitivity (78%−100%) increased as the lesion got deeper and at any scanning angles. This finding is similar to previous studies with natural non-cavitated occlusal and smooth surfaces lesions [7,11]. In this current study, specificity ranged from 66 to 87% and the area under the Receiver Operating Characteristic curve (AUC) ranged from 0.86 to 0.92 at varying scanning angles. Intraclass correlation coefficients (ICC) in this current study (0.89–0.99) demonstrated good to excellent repeatability [33]. Generally, the variability in motor execution makes it virtually impossible to exactly repeat actions [34]. When scanning occlusal surface sites ranging from sound to non-cavitated

Table 1
Sensitivity, specificity, area under the ROC curve (AUC) and intraclass correlation coefficient (ICC) for different scanning angles.

Angle	Sensitivity (%)				Specificity (%)	AUC	ICC
	Overall	μ-CT=1	μ-CT=2	μ-CT=3			
20° to buccal	81	42	100	100	66	0.89	0.96
10° to buccal	89	67	100	100	87	0.91	0.97
Buccal-Lingual 90°	86	59	100	100	79	0.91	0.96
10° to lingual	86	58	100	100	83	0.91	0.99
20° to lingual	89	67	100	100	70	0.90	0.94
20° to occlusal	83	58	92	100	66	0.87	0.95
10° to occlusal	78	42	92	100	71	0.86	0.94
Occlusal-Cervical 90°	89	67	100	100	78	0.92	0.94
10° to cervical	87	67	92	100	71	0.90	0.89
20° to cervical	89	75	92	100	71	0.88	0.89

μ-CT=1: lesion in the outer half of the enamel, μ-CT=2: lesion in the inner half of the enamel but not extending beyond the dentin-enamel junction, and μ-CT=3: lesions in the outer one third of the dentin. There were no significant differences among angles for overall sensitivity ($p>0.12$), sensitivity for μ-CT=1/μ-CT=2/μ-CT=3 ($p>0.10$, $p>0.50$, $p=1.00$), specificity ($p>0.06$), AUC ($p>0.18$), or ICC ($p>0.06$).

Table 2a
Pearson correlation coefficients between PTR/LUM values and lesion depths/length on different μ-CT slices.

μ-CT Depth	μ-CT Slice	PTR/LUM Scanning Angle									
		20° to buccal	10° to buccal	buccal-lingual 90°	10° to lingual	20° to lingual	20° to occlusal	10° to occlusal	occlusal-cervical 90°	10° to cervical	20° to cervical
Slice-Mean	Buccal	−0.05	−0.11	0.00	0.01	0.00	0.00	−0.07	−0.03	−0.18	−0.06
	Middle	0.60*	0.55*	0.51*	0.57*	0.53*	0.65*	0.57*	0.63*	0.52*	0.56*
	Lingual	0.43	0.43	0.44	0.46	0.39	0.42	0.43	0.34	0.26	0.29
	Occlusal	0.33	0.37	0.29	0.29	0.24	0.43	0.35	0.34	0.38	0.32
	Cervical	0.50*	0.48*	0.54*	0.54*	0.43	0.46	0.51*	0.42	0.34	0.35
Slice-Maximum	Buccal	0.19	0.14	0.07	0.13	0.19	0.31	0.15	0.31	0.17	0.23
	Middle	0.60*	0.55*	0.52*	0.58*	0.55*	0.64*	0.57*	0.63*	0.51*	0.54*
	Lingual	0.55*	0.53*	0.46	0.51*	0.51*	0.63*	0.53*	0.60*	0.46	0.51*
	Occlusal	0.35	0.36	0.21	0.29	0.25	0.52	0.32	0.42	0.42	0.46
	Cervical	0.41	0.37	0.45	0.45	0.42	0.39	0.43	0.38	0.25	0.29
All-Mean	All slices	0.50*	0.47*	0.48*	0.51*	0.46	0.55*	0.49*	0.49*	0.36	0.42
All-Maximum	All slices	0.60*	0.55*	0.48*	0.56*	0.53*	0.65*	0.56*	0.63*	0.50*	0.55*
Deepest lesion		0.67*	0.62*	0.56*	0.61*	0.60*	0.70*	0.61*	0.65*	0.57*	0.62*

Correlations with * were statistically significant ($p<0.05$). Slice-Mean/Maximum: mean/maximum lesion depth/length on μ-CT images for each slice. All-Mean/Maximum: mean/maximum lesion depth/length on μ-CT images for all slices of one study tooth. Deepest lesion: deepest lesion depth of the study tooth on μ-CT images, which might not be in the center of lesion.

Table 2b
Pearson correlation coefficients between PTR/LUM values and lesion depth/sound tissue thickness under lesion (LD/ST-Ratio).

LD/ST-Ratio	μ-CT Slice	PTR/LUM Scanning Angle									
		20° to buccal	10° to buccal	buccal-lingual 90°	10° to lingual	20° to lingual	20° to occlusal	10° to occlusal	occlusal-cervical 90°	10° to cervical	20° to cervical
Slice-Mean	Buccal	−0.05	−0.11	0.01	0.01	0.00	0.00	−0.07	−0.04	−0.18	−0.06
	Middle	0.60*	0.56*	0.51*	0.57*	0.53*	0.65*	0.57*	0.64*	0.52*	0.56*
	Lingual	0.45	0.45	0.45	0.47*	0.40	0.43	0.45	0.36	0.28	0.30
	Occlusal	0.34	0.37	0.30	0.29	0.24	0.43	0.35	0.34	0.38	0.32
	Cervical	0.50*	0.48*	0.55*	0.54*	0.44	0.46	0.52*	0.43	0.35	0.35
Slice-Maximum	Buccal	0.23	0.19	0.10	0.16	0.22	0.35	0.19	0.36	0.22	0.28
	Middle	0.61*	0.56*	0.53*	0.59*	0.55*	0.65*	0.58*	0.64*	0.52*	0.55*
	Lingual	0.56*	0.56*	0.48*	0.53*	0.52*	0.65*	0.56*	0.62*	0.48*	0.53*
	Occlusal	0.35	0.36	0.21	0.29	0.25	0.52*	0.32	0.43	0.42	0.47
	Cervical	0.40	0.37	0.45	0.44	0.41	0.38	0.42	0.38	0.24	0.28
All-Mean	All slices	0.50*	0.47*	0.48*	0.52*	0.46	0.54*	0.49*	0.49	0.36	0.42
All-Maximum	All slices	0.61*	0.57*	0.49*	0.56*	0.54*	0.66*	0.57*	0.65*	0.52*	0.56*
Deepest lesion		0.70*	0.66*	0.59*	0.64*	0.63*	0.74*	0.64*	0.69*	0.61*	0.65*

Correlations with * were statistically significant ($p<0.05$). Slice-Mean/Maximum: mean/maximum LD/ST-Ratio on μ-CT images for each slice. All-Mean/Maximum: mean/maximum LD/ST-Ratio on μ-CT images for all slices of one study tooth. Deepest lesion: largest LD/ST-Ratio of the study tooth on μ-CT images at the deepest lesion site.

lesions *in vitro*, the lower reproducibility (ICC 0.48) founded by Jallad et al. [12]. This might be due to hand-held teeth samples. The hand-held setting might induce some degree increments in angle and miss the middle of the lesion. The ideal experimental setting is to fix the position and scan at the same location every time.

4.3. Contribution of lesion depth, sound tissue thickness under the lesion to PTR/LUM value

In the current study, the maximum lesion depth showed no significant differences (from 513 μm to 725 μm) among scanning angles. Correlation between the maximum lesion depth and PTR/LUM value ranged between 0.57 and 0.70 among all scanning angles. Similar correlations were reported previously [4,12,35]. Abrams et al. [7] found the correlation coefficient was 0.84 between caries lesion depth and PTR/LUM value when scanning caries on smooth and occlusal surfaces. The lesion distribution was: out of total 20 samples, 6 samples showed caries lesion depths deeper than 800 μm, 11 samples showed caries lesion depths shallower than 800 μm, while 3 samples were sound. In this current study, lesion depths among different angles were shallower than 800 μm (Fig 2a). The heterogeneity of caries detection studies makes comparisons between studies difficult. Study designs might differ with respect to patients/tooth samples selection, use of diagnostic and reference methods, calibration, blinding and data reporting [36]. Dental caries development always accompanies mineral loss [37]. When scanning dental caries, the amorphous mineral at boundary of the lesion could effectively increase the scattering coefficient and then decrease the thermal wave diffusion length [21]. This process may have resulted in the observed increasing in PTR-amplitude (the strength of the converted heat) and PTR-phase (the time delay of the converted heat to reach the surface). Simultaneously, lesion development increased mineral loss and then decreased LUM signals, before finally increasing PTR/LUM value [32]. The current study found similarities in the correlations between PTR/LUM value and lesion depth and between PTR/LUM value and LD/ST-Ratio, indicated that the thickness of sound tissue under the lesion did not impact the relationship of PTR/LUM value with lesion depth. Raw PTR/LUM values were calculated as follows: Raw PTR/LUM value=C(PTR-amplitude × PTR- phase)/(LUM-amplitude × LUM- phase), where C indicates a device calibration constant, LUM amplitude indicates the strength of the converted luminescent light) and LUM phases indicates the time delay of the converted luminescent light. Then it was converted into graduated PTR/LUM values (Canary Number: 0-100) based on an empirical semi-logarithmic plot [5,20]. The sound surface PTR/LUM values (<20) were converted based on the raw PTR/LUM value driving from sound enamel and dentine signals. Although healthy sound crystal tissue contributes to raw PTR/LUM value [4] and might decrease raw PTR/LUM value [17], because of weak PTR/LUM signal changes from sound tissue, PTR/LUM value are mostly driven by PTR/LUM signal from caries.

5. Conclusions

In conclusion, within the limitations of this current study, varying scanning angle up to 20° from perpendicular to the surface might have some impact on the PTR/LUM values; however, varying scanning angle up to 20° may not impact the PTR/LUM performance of caries detection. There is a moderate correlation between PTR/LUM value and lesion depth when scanning non-cavitated dental caries. Lesion depth contributed dominantly to PTR/LUM value, whereas sound tissue under the lesion may not have significantly impacted PTR/LUM value.

CRediT authorship contribution statement

Haixia Xing: Conceptualization, Funding acquisition, Writing – original draft. **George J. Eckert:** Formal analysis, Conceptualization, Writing – original draft. **Masatoshi Ando:** Conceptualization, Funding acquisition, Writing – original draft.

Declaration of Competing Interest

The authors declare that they have no known competing financial interests or personal relationships that could have appeared to influence the work reported in this paper.

Acknowledgments

The authors declare no potential conflicts of interest with respect to the authorship and/or publication of this article.

References

[1] C.L. Darling, G.D. Huynh, D. Fried, Light scattering properties of natural and artificially demineralized dental enamel at 1310nm, J. Biomed. Opt. 11 (3) (2006) 34023, https://doi.org/10.1117/1.2204603.
[2] R.J. Jeon, A. Matvienko, A. Mandelis, S.H. Abrams, B.T. Amaechi, G. Kulkarni, Detection of interproximal demineralized lesions on human teeth *in vitro* using frequency-domain infrared photothermal radiometry and modulated luminescence, J. Biomed. Opt. 12 (3) (2007), 034028, https://doi.org/10.1117/1.2750289.
[3] R.J. Jeon, A. Mandelis, V. Sanchez, S.H. Abrams, Nonintrusive, noncontacting frequency-domain photothermal radiometry and luminescence depth profilometry of carious and artificial subsurface lesions in human teeth, J. Biomed. Opt. 9 (4) (2004) 804–819, https://doi.org/10.1117/1.1755234.
[4] C.F. Lena Nicolaides, A. Mandelis, S.H. Abrams, Quantitative dental measurements by use of simultaneous frequency-domain laser infrared photothermal radiometry and luminescence, Appl. Opt. 41 (4) (2002) 768–777.
[5] J.D. Silvertown, S.H. Abrams, K.S. Sivagurunathan, J. Kennedy, J. Jeon, A. Mandelis, A. Hellen, W. Hellen, G. Elman, R. Ehrlich, R. Chouljian, Y. Finer, B. T. Amaechi, Multi-centre clinical evaluation of photothermal radiometry and luminescence correlated with international benchmarks for caries detection, Open. Dent. J. 11 (2017) 636–647, https://doi.org/10.2174/1874210601711010636.
[6] R.J. Jeon, C. Han, A. Mandelis, V. Sanchez, S.H. Abrams, Diagnosis of pit and fissure caries using frequency-domain infrared photothermal radiometry and modulated laser luminescence, Caries Res. 38 (6) (2004) 497–513, https://doi.org/10.1159/000080579.
[7] S.H. Abrams, K.S. Sivagurunathan, J.D. Silvertown, B. Wong, A. Hellen, A. Mandelis, W.M.P. Hellen, G.I. Elman, S.M. Mathew, P.K. Mensinkai, B. T. Amaechi, Correlation with caries lesion depth of the canary system, DIAGNOdent and ICDAS II, Open. Dent. J. 11 (2017) 679–689, https://doi.org/10.2174/1874210601711010679.
[8] J. Jan, W.Z. Wan Bakar, S.M. Mathews, L.O. Okoye, B.R. Ehler, C. Louden, B. T. Amaechi, Proximal caries lesion detection using the canary caries detection system: an *in vitro* study, J. Investig. Clin. Dent. 7 (4) (2016) 383–390, https://doi.org/10.1111/jicd.12163.
[9] K. Herzog, M. D'Elia, A. Kim, R.L. Slayton, Pilot study of the canary system use in the diagnosis of approximal carious lesions in primary molars, Pediatr. Dent. 37 (7) (2015) 525–529.
[10] B.T. Amaechi, L.O. Okoye, E. Uzamere, S.M. Mathews, W.Z.W. Bakar, J. Jan, Clinical trial of the canary system for proximal caries detection: a comparative study, Curr. J. Appl. Sci. Technol. 40 (35) (2021) 38–50.
[11] H. Xing, G.J. Eckert, M. Ando, Detection ability and direction effect of photothermal-radiometry and modulated-luminescence for non-cavitated approximal caries, J. Dent. 90 (2019), 103221, https://doi.org/10.1016/j.jdent.2019.103221.
[12] M. Jallad, D. Zero, G. Eckert, A. Ferreira Zandona, *In vitro* detection of occlusal caries on permanent teeth by a visual, light-induced fluorescence and photothermal radiometry and modulated luminescence methods, Caries Res. 49 (5) (2015) 523–530, https://doi.org/10.1159/000437214.
[13] T.E. Abrams, S.H. Abrams, K.S. Sivagurunathan, J.D. Silvertown, W.M.P. Hellen, G. I. Elman, B.T. Amaechi, *In vitro* detection of caries around amalgam restorations using four different modalities, Open. Dent. J. 11 (2017) 609–620, https://doi.org/10.2174/1874210601711010609.
[14] J.G. Lena Nicolaides, A. Mandelis, S.H. Abrams, Dental depth profilometry using simultaneous frequency-domain infrared photothermal radiometry and laser luminescence for the diagnosis of dental caries, Proc. SPIE 4249 (2001) 79–86.
[15] A.M. Jose, A. Garcia, S.H. Abrams, A. Matvienko, Photothermal radiometry and modulated luminescence: applications for dental caries detection. Handbook of Biophotonics, Vol. 2: Photonics for Health Care First Edition, Wiley-VCH Verlag GmbH & Co. KGaA, 2012, pp. 1047–1052.
[16] R.J. Jeon, A. Hellen, A. Matvienko, A. Mandelis, S.H. Abrams, B.T. Amaechi, *In vitro* detection and quantification of enamel and root caries using infrared photothermal radiometry and modulated luminescence, J. Biomed. Opt. 13 (3) (2008), 034025, https://doi.org/10.1117/1.2942374.
[17] A. Hellen, A. Mandelis, Y. Finer, B.T. Amaechi, Quantitative evaluation of the kinetics of human enamel simulated caries using photothermal radiometry and modulated luminescence, J. Biomed. Opt. 16 (7) (2011), 071406, https://doi.org/10.1117/1.3564909.

[18] M. Ando, G.J. Eckert, G.K. Stookey, D.T. Zero, Effect of imaging geometry on evaluating natural white-spot lesions using quantitative light-induced fluorescence, Caries Res. 38 (1) (2004) 39–44, https://doi.org/10.1159/000073919.
[19] S. Abrams, Overcoming the challenges of caries detection using the canary system, Oral Health 101 (12) (2011) 17–22.
[20] A. Hellen, A. Matvienko, A. Mandelis, Y. Finer, B.T. Amaechi, Optothermophysical properties of demineralized human dental enamel determined using photothermally generated diffuse photon density and thermal-wave field, Appl. Opt. 49 (36) (2010) 6938–6951.
[21] A.F. Dayo, B.T. Amaechi, M. Noujeim, S.T. Deahl, P. Gakunga, R. Katkar, Comparison of photothermal radiometry and modulated luminescence, intraoral radiography, and cone beam computed tomography for detection of natural caries under restorations, Oral. Surg. Oral. Med. Oral. Pathol. Oral. Radiol. 1 129 (5) (2020) 539–548, https://doi.org/10.1016/j.oooo.2019.09.006.
[22] J.D. Silvertown, B.P.Y. Wong, K.S. Sivagurunathan, S.H. Abrams, J. Kirkham, B. T. Amaechi, Remineralization of natural early caries lesions *in vitro* by P11 -4 monitored with photothermal radiometry and luminescence, J. Investig. Clin. Dent. 8 (4) (2017), https://doi.org/10.1111/jicd.12257.
[23] J. Kim, A. Mandelis, A. Matvienko, S. Abrams, B.T. Amaechi, Detection of dental secondary caries using frequency-domain infrared photothermal radiometry (PTR) and modulated luminescence (LUM), Int. J. Thermophys. 33 (10–11) (2012) 1778–1786, https://doi.org/10.1007/s10765-012-1322-x.
[24] O. Fejerskov, Pathology of Dental caries, Dental Caries, The Disease and Its Clinical Management, 3rd Edition, Wiley Oxford, Blackwell, 2015, pp. 49–81.
[25] N. Abogazalah, G.J. Eckert, M. Ando, *In vitro* performance of near infrared light transillumination at 780-nm and digital radiography for detection of non-cavitated approximal caries, J. Dent. 63 (2017) 44–50, https://doi.org/10.1016/j.jdent.2017.05.018.
[26] E. Stratigaki, F.N. Jost, J. Kuhnisch, F. Litzenburger, A. Lussi, K.W. Neuhaus, Clinical validation of near-infrared light transillumination for early proximal caries detection using a composite reference standard, J. Dent. 103S (2020), 100025, https://doi.org/10.1016/j.jjodo.2020.100025.
[27] J.W. Osborne, Evaluation of previous assessments of prism directions in human Enamel, J. Dent. Res. 47 (1968) 217–222.
[28] J.W. Osborne, Directions and interrelations of enamel prisms from the sides of human teeth, J. Dent. Res. 47 (1968) 223–232.
[29] C.P. Fernandes, O. Chevitarese, The orientation and direction of rods in dental enamel, J. Prosthet. Dent. 65 (1991) 793–800.
[30] A. Boyde, Enamel tissue and cavity margins, Oper. Dentl. 1 (1976) 13–20.
[31] O.C. Claudio Pinheiro Fernandes, The orientation and direction of rods in dental enamel, J. Prosthet. Dent. 65 (1991) 793–800.
[32] A. Hellen, A. Mandelis, Y. Finer, B.T. Amaechi, Quantitative remineralization evolution kinetics of artificially demineralized human enamel using photothermal radiometry and modulated luminescence, J. Biophoton. 4 (11–12) (2011) 788–804, https://doi.org/10.1002/jbio.201100026.
[33] T.K. Koo, M.Y. Li, A guideline of selecting and reporting intraclass correlation coefficients for reliability research, J. Chiropr. Med. 15 (2) (2016) 155–163, https://doi.org/10.1016/j.jcm.2016.02.012.
[34] J. Komar, L. Seifert, R. Thouvarecq, What variability tells us about motor expertise: measurements and perspectives from a complex system approach, Mov. Sport. Sci/Sci. Mot. (89) (2015) 65–77, https://doi.org/10.1051/sm/2015020.
[35] R.J. Jeon, L.V. Wang, A. Hellen, A. Matvienko, A. Mandelis, S.H. Abrams, B. T. Amaechi, Experimental investigation of demineralization and remineralization of human teeth using infrared photothermal radiometry and modulated luminescence, Proc. SPIE. BIOS 6856 (2008) 68560B, https://doi.org/10.1117/12.763807.
[36] J. Kuhnisch, M. Janjic Rankovic, S. Kapor, I. Schuler, F. Krause, S. Michou, K. Ekstrand, F. Eggmann, K.W. Neuhaus, A. Lussi, M.C. Huysmans, Identifying and avoiding risk of bias in caries diagnostic studies, J. Clin. Med. 10 (15) (2021), https://doi.org/10.3390/jcm10153223.
[37] K.P. Preston, S.M. Higham, P.W. Smith, The efficacy of techniques for the disinfection of artificial sub-surface dentinal caries lesions and their effect on demineralization and remineralization *in vitro*, J. Dent. 35 (6) (2007) 490–495, https://doi.org/10.1016/j.jdent.2007.01.006.